Dynamical Tests on Fiber Optic Data Taken from the Riser Section of a Circulating Fluidized Bed

Emily M. Taylor, Christopher P. Guenther, Ronald W. Breault, US Department of Energy, National Energy Technology Laboratory, Morgantown, WV 26507, USA

Abstract

Dynamical tests have been applied to fiber optic data taken from a cold-flow circulating fluidized bed to characterize flow conditions, identify three time and/or length scales (macro, meso, and micro), and understand the contribution these scales have on the raw data. The characteristic variable analyzed is the raw voltage signal obtained from a fiber-optic probe taken at various axial and radial positions under different loading conditions so that different flow regimes could be attained. These experiments were carried out with the bed material of 812 μm cork particles. The characterization was accomplished through analysis of the distribution of the signal through the third and fourth moments of skewness and excess kurtosis. A generalization of the autocorrelation function known as the average mutual information function was analyzed by examining the function's first minimum, identifying the point at which successive elements are no longer correlated. Further characterization was accomplished through the correlation dimension, a measure of the complexity of the attractor. Lastly, the amount of disorder of the system is described by a Kolmogorov-type entropy estimate. All six aforementioned tests were also implemented on ten levels of detail coefficients resulting from a discrete wavelet transformation of the same signal as used above. Through this analysis it is possible to identify and describe micro (particle level), meso (clustering or turbulence level), and macro (physical or dimensional level) length scales even though some literature considers these scales inseparable [6]. This investigation also used detail wavelet coefficients in conjunction with ANOVA analysis to show which scales have the most impact on the raw signal resulting from local hydrodynamic conditions.

Introduction

Deterministic chaos theory has recently been used as a tool to analyze the dynamics within gas-solid systems, such as fluidized beds. This theory has been used for the purpose of examining scale-up effects [8, 12], identifying regime changes [3, 17, 18], characterizing fluidization [5], and determining how changes in conditions affect dynamics [4, 10].

Three scales can be identified within a fluidized bed: the macroscale representing the physical or global aspects of the unit, the mesoscale expressing the clusters and their interactions, and microscale of individual particle behavior. Bai et al.[1] and Ji et al. [11] examined the three scales by observing three separate time series collected from three separate probes. A single time series decomposed through wavelet decomposition into series of detail and approximation coefficient was utilized to identify the three scales by Zhao and Yang [20] and Wu et al. [16]. This method of decomposition allows information from different frequency components to be analyzed separately.

A majority of the current work have used deterministic chaos or wavelets techniques to analyze signals from a bubbling bed where the regime transitions and scales are well-defined. The objective of this work is to extend and add upon the characteristic techniques and regime and scale identification to a circulating fluidized bed, where these transitions are more subtle.

It was concluded by Zhao and Yang [20] and implemented by many others that characterization of a fluidized bed cannot be accomplished through a single test or approach. Therefore, multiple tests are being used in the current work on both the raw and wavelet data. In general, the wavelet data served to examine each scale independently. Combine this with the examination of the raw data and based on trends and ANOVA results, it can be concluded which scale most contributes to the changes seen within the raw data.

Experimental

The experimental unit is a cold flow circulating fluidized bed located at National Energy Technology Laboratory (NETL) in Morgantown, WV. It consists of a riser 15.3 m high and 0.3 m diameter and a 0.25 m diameter standpipe. The transfer leg is a loopseal with a 0.23 m diameter allowing the solids to enter the riser from a side port 0.27 m above the distributor. Cork with an average size of 812 μm was the test bed material. Solids circulation rate (Ms) and gas velocity (Ug) was varied independently; studied values are shown in table 1.

Table 1
Operating Conditions

Ug (m/s)	Ms (kg/h)	Load Ratio
4.6	907.2	0.62
5.5	2721.6	1.55
4.6	2721.6	1.86
3.8	2721.6	2.25
4.6	4535.9	3.10

Data was also obtained for three separate axial locations and five radial positions. Axial locations were chosen in an effort to characterize the acceleration zone (3.9m), the fully developed zone (8.3m), and deceleration zone (12.1m). Radial positions were chosen as the midpoint of five equal area circles within the riser. These positions will be referred to as P0, P1, P2, P3, and P4 and represent distances of 0.12, 0.07, 0.05, 0.03, and 0.01 m from the wall, respectively.

The data was acquired using a multi-fiber optical reflective probe developed by Vector Scientific instruments. It consists of two fiber bundles located on the same vertical line. Each bundle is composed of 150 randomly distributed of each transmitting and receiving fibers. A light emitting diode (LED) transmits light through the transmitting half of the fibers, where upon hitting particle(s) in the riser will be reflected back to the probe. The intensity of the reflected light depends on the concentration, size distribution, composition, and shape of the particles. The sampling rate was12.5 kHz and data was collected for 61.536 sec.

Calculations

Various statistics can be used to describe the distribution of a dataset. Higher order moments of skewness and excess kurtosis are of interest. Skewness is a measure of the asymmetry of the distribution and excess kurtosis quantifies the peakedness. As a point of reference, a Gaussian distribution has skewness and kurtosis values of zero.

Also of interest is the amount of dependence the signal has with itself, or amount of memory a signal possesses. The AMI function is a general measure of dependence that can detect both linear and non-linear correlations. Its first minimum represents the point at which successive elements are no longer correlated.

The two chaotic statistics used here are the correlation dimension which is a dimensionless number that represents the complexity of the signal, and the correlation entropy which is a measure of the predictability. Both values are calculated from the reconstructed attractor most commonly computed through Takens' delay embedding theorem [15]. The correlation dimension can be interpreted as the number of degrees of freedom that dominate

the dynamic behavior of the system. Entropy can be interpreted as a quantitative measure of the amount of information needed to predict the value of an observation within a certain precision.

Statistics will also be computed for the series of coefficients resulting from a discrete wavelet transformation (DWT). This process involves passing the signal *f(x)* through a low and high pass filter multiple times to examine the different levels of detail of *f(x)* independently. The output of the low pass filter known as the approximation coefficients, a^j, form a smoother and smoother version of the raw signal. The detail lost by going to the next higher level is captured in the detail coefficients, d^j, output of the high-pass filter. Each filter and level of decomposition represents a different frequency band, given by

$$d^j : \left[2^{-(j+1)} f_s, 2^{-j} f_s\right] \qquad a^j : \left[0, 2^{-(j+1)} f_s\right] \quad (1)$$

where f_s represents the sampling frequency. Therefore, a reconstruction of the original signal is accomplished with the summation of the detail coefficients at all levels and the highest level of approximation. In this work the detail coefficients up to level $j = 10$ are considered. The Daubechies mother wavelet was utilized here for its simplicity, compact support, perfect reconstruction, orthogonality, highest number of vanishing moments, *L*, for a given support width and popularity within the literature [2, 4, 8, 9, 16, 20].

Scale Identification

A ten level DWT was performed on the raw signal to examine the different frequency bands and determine which scale, micro, meso, or macro, they represent. It is desired to determine which phenomena within the CFB these bands are able to characterize.

Figure 1 presents the trend of the first minimum at increasing scales for three randomly chosen combinations of independent variables. At the first half of the scales the first minimum value remains low. Once the sixth level is attained the amount of memory within the decomposed signal begins to significantly increase and steadily increases to the maximum scale of d10. This trend can be explained by the occurrence of a change within the CFB system will not be absorbed by the macro scale as quickly as the micro or meso scales. A greater number of time increments will then be necessary before elements are no longer correlated at the macroscale, leading to a larger value for the first minimum. Therefore, the examination of the first minimum of the AMI function indicates a boundary between the macro and meso scales with d6-d10 being identified as the macro scale.

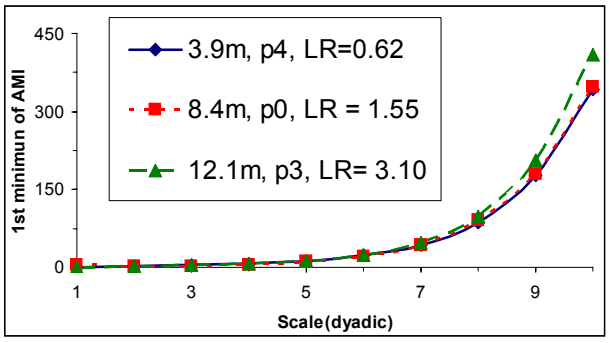

Figure 1-First minimum of the AMI function of the detail coefficient series (d1-d10) for three representative data sets

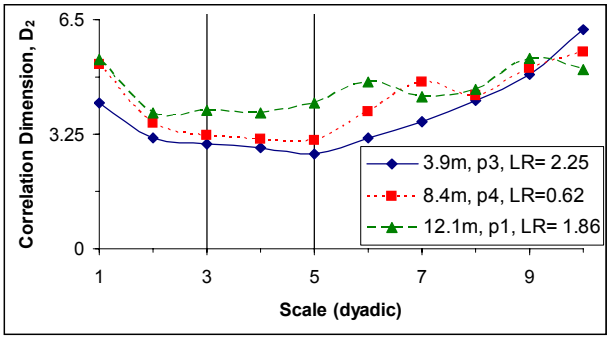

Figure 2- Correlation dimension, D_2, of the detail coefficient series (d1-d10) for three representative data sets.

A plot of the correlation dimension as a function of the dyadic scale for three representative time series can be seen in figure 2. For the lowest two scales, the dimension value decreases for all series. At the third detail level, the estimates level off and do not vary until d6 where the values begin to increase and continue to do so until d10. It has already been determined that the macro scale begins at d6, but the first shift in trends indicate that d1 and d2 represent the micro scale, or individual particle interactions, and d3-d5 characterizes the meso scale, or clusters. This is consistent with the view of larger changes in the high frequency fluctuations due to the random movement of particles which would correspond to higher dimensionality.

With a sampling frequency of 12.5 kHz and equation 1, it can be concluded the frequency band which corresponds to the mesoscale is (195 Hz, 1563 Hz). This implies that the clustering is occurring at time scales between 0.00064 s and 0.00512 s. Guenther and Breault [9] found clusters to occur within similar time scales for cork bed material.

Results and Discussion

The characterization of flow regimes, phenomena within scales, and the dominant contributing scale to the raw signal can be accomplished with the examination of a combination of tests on both the raw voltage signal and detail wavelet coefficients. Many plots will be presented as a group and will follow the order of the circles shown in figure 3. Here, changes in the solids circulation rate (Ms) are along the abscissa and the riser gas velocity (Ug) along the ordinate. The relative size of the circles in figure 3 represents load ratio. A dilute upflow regime was seen in the case with the least amount of loading and smallest Ms value. For Ms = 2721.6 kg/hr, the larger two values of gas velocity exhibit behavior within the core annular flow regime, and the lowest Ug value operates in the fast fluidization regime. The point with the largest amount of loading and the highest Ms can demonstrate characteristics within the fast fluidization and core annular regimes. The lines in figure 3 are shown to classify the regime in which the points studied in this work are operating and do not represent boundaries for the flow regimes of values not plotted here. These divisions were suggested by the solids velocity in [21] and riser pressure profiles in [13]. Since the heaviest loaded case has been known to show behavior within both core annular and fast fluidization, the boundary can be represented by either the solid or dashed line.

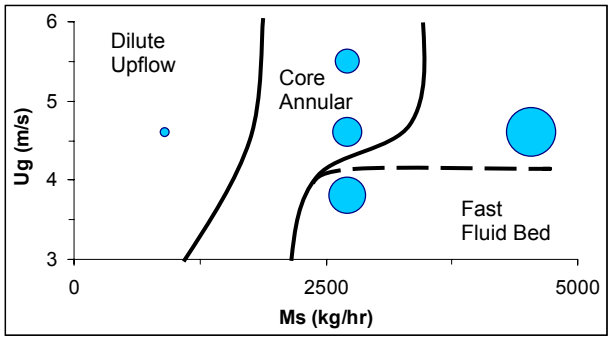

Figure 3- The structure of most groups of graphs in this section.

For the raw voltage signal, the first minimum of the AMI function is plotted against radial position at varying axial locations in figure 4. The trend for most cases is a steady increase from the center (p0) to the wall (p4). Since it takes more time steps for elements to become uncorrelated, this implies that there is more memory in the raw data at the wall. This increase becomes more pronounced as the load ratio increases. Dilute upflow has the least amount of memory overall. The discrepancy between the lower elevation (3.9 m) and the other axial locations is largest while operating at the highest two load ratios. A characterization of the fast fluidization is the “S” shaped pressure profile which is indicative of and exhibits “classical Yerushalmi [19] behavior” in the dense region at the bottom of the riser. Figure 4 indicates that

the two heaviest loaded cases are within the fast fluidization regime. The two highest load ratios also show that fast fluidization and core-annular can exist simultaneously in the riser at two different elevations which explains the ambiguity of the dashed line in figure 3. By examining the incremental differential pressure profiles, this transition is not as obvious, providing an advantage of the AMI over incremental pressure measurements. If the correlation dimension, D_2, is plotted in the same manner, it can be seen that the complexity of the attractor is also greatest at the wall of the riser. The transition between fast fluid and core annular is also present, but not as well-defined.

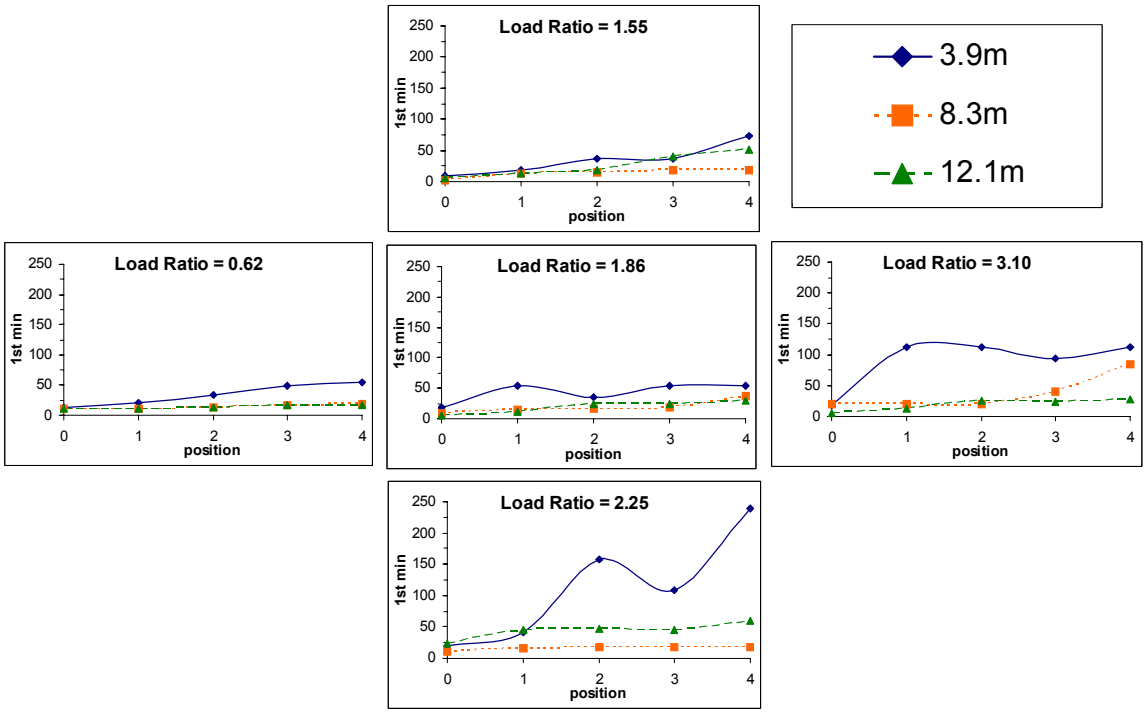

Figure 4- 1st min of the AMI function versus radial position for the raw voltage data at three axial locations.

Figure 5 characterizes the distribution of the raw signal with excess kurtosis by plotting it against the radial position at each axial location with a different graph for each load ratio. A similar analysis was also performed for the skewness, but because of space limitations not shown here. None of the distributions are statistically equivalent to the Gaussian distribution with skewness and excess kurtosis values of 0 using the standard error of skewness of $SES = \sqrt{\frac{6}{n}}$ and kurtosis of $SEK = \sqrt{\frac{24}{n}}$ defined in [14]. All cases are positively skewed i.e. have a longer tail in the positive direction because the fiber optic probe measures the intensity of reflected light and this intensity is low due to the frequently passing voids. A majority of the distributions are also leptokurtic (kurtosis > 0) which can be seen in figure 5. At the heavier loaded cases, more platykurtic (kurtosis < 0) distributions occur. The trend is for the distribution to approach Gaussian closer to the wall in relation to both the skewness and kurtosis. One exception to this trend is the dilute upflow case (LR = 0.62) which remains consistently positively skewed and leptokurtic across the radius. This boundary for dilute upflow is also present in the skewness plots; however, not as pronounced as that seen for the kurtosis.

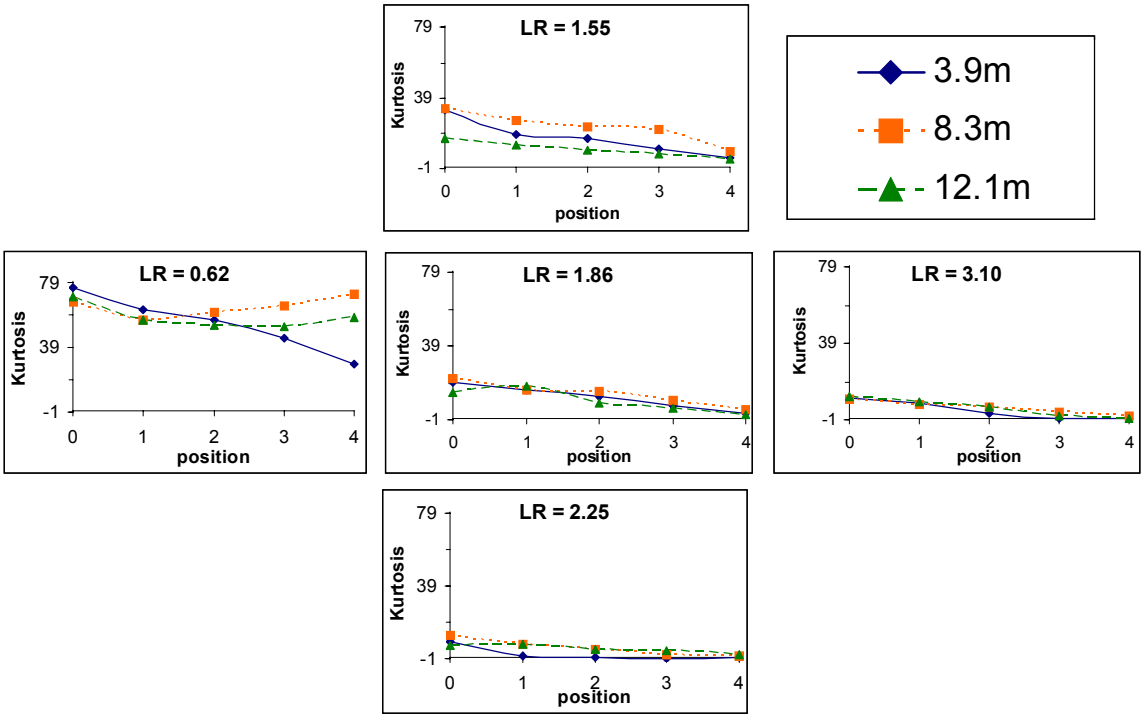

Figure 5- Excess kurtosis versus radial position for the raw voltage data at three axial locations.

Since the detail coefficients that relate to micro, meso, and macro scales have been identified, it is possible to analyze each scale independently by averaging over the corresponding detail levels (i.e. d1 and d2 for micro, d3-d5 for meso, and d6-d10 for macro). The result of doing this for the excess kurtosis for at 8.3m are plotted against the radial position at varying scales with a separate plot for each load ratio in figure 6. High kurtosis values of detail coefficients can indicate intermittency caused by high frequency fluctuations from particle movements [2]. The fact that the microscale is always the most intermittent is further indication that this scale is capturing particle behavior. For the micro and meso scales, as the load ratio increases the kurtosis value decreases with a considerable decrease going from the lowest load ratio to all others indicating that detail wavelet coefficients at these scales can be used to identify a boundary for dilute upflow. To further quantify these results a separate ANOVA was performed at each scale for the data at all three elevations with table 2 indicating which independent variables were significant. The value in parenthesis of each heading indicates the adjusted R^2 value, a measure of the amount of variability explained by the model. Since the

Table 2

ANOVA for response variable of excess kurtosis.

Scale (Adjusted R^2)	micro (.42)	meso (.70)	macro (.14)	raw (.95)
Axial	x			
Ug		x	x	x
Ms	x	x	x	x
Radial	x	x		x
Axial*Ug				
Axial*Ms				
Axial*Radial				x
Ug*Radial				
Ms*Radial			x	
Axial^2				x
Ug^2				
Ms^2	x	x		x
Radial^2				

*x indicates significant at a 0.01 level of significance.

macroscale did not pick up on the regime transition and the model is such a poor fit (R_a^2 = 0.14), nothing can be concluded about the macroscale from examination of the kurtosis. In comparing the significant terms of the ANOVAs in table 2 of each scale to that of the raw, it can be seen that the scale that has the greatest influence on the excess kurtosis of the raw data is the mesoscale.

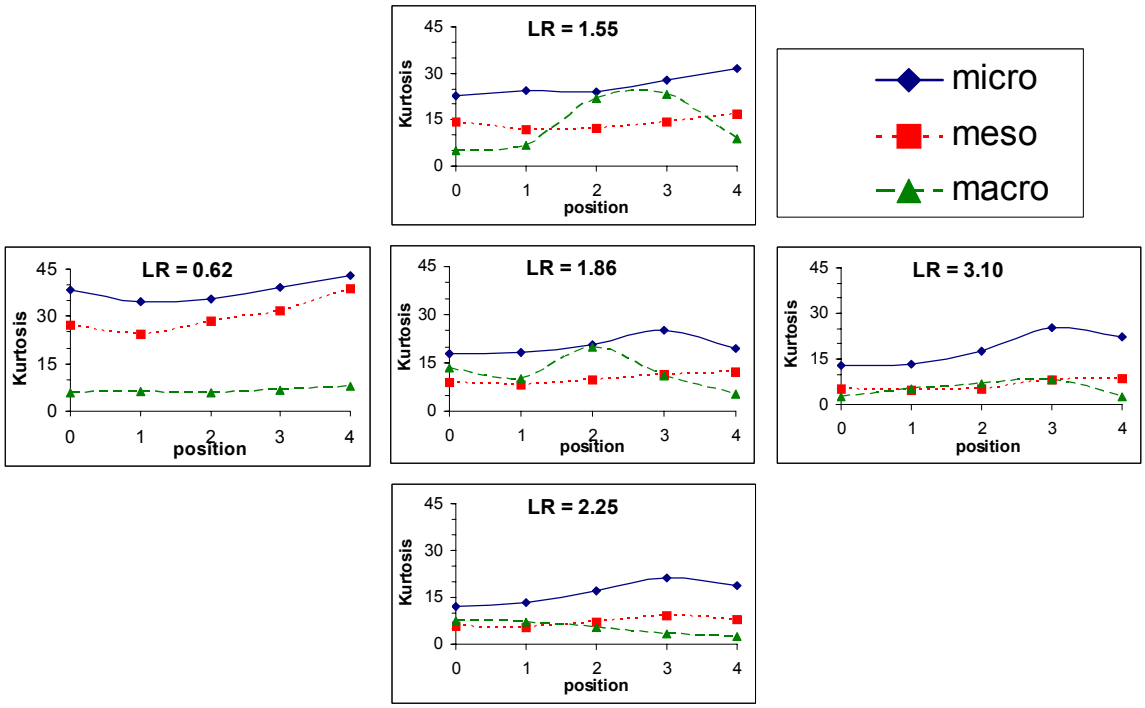

Figure 6 - Average excess kurtosis values versus radial position at the 8.3m elevation for each scale identified with wavelet analysis.

Table 3
ANOVA for response variable of correlation dimension.

Scale (Adjusted R^2)	micro (.19)	meso (.75)	macro (.18)	raw (.80)
Axial	x	x		
Ug		x		x
Ms		x		x
Radial		x	x	x
Axial*Ug				
Axial*Ms			x	
Axial*Radial				x
Ug*Radial			x	
Ms*Radial				
Axial^2				
Ug^2		x		x
Ms^2				
Radial^2	x	x	x	x

*x indicates significant at 0.01 level of significance

Correlation entropy, h_2, as a function of radial position can be seen for each scale at the 8.3m elevation in figure 7. For almost every set of points, the mesoscale has the lowest entropy value. In terms of all other independent variables, there is no noticeable trend from these graphs. This implies that the meso scale has the lowest rate of information loss, or the most memory. For the raw data, it was shown in figure 4 that the first minimum of the AMI function was greatest at the wall and thus the amount of memory increased towards this wall. This implies that the mesoscale has more influence at the wall than at the center. Furthermore, from table 3 it can be concluded that since the model with the response variable of correlation dimension for the raw data most closely agrees with the mesoscale, it is this scale that is dominating the dynamics of the raw signal.

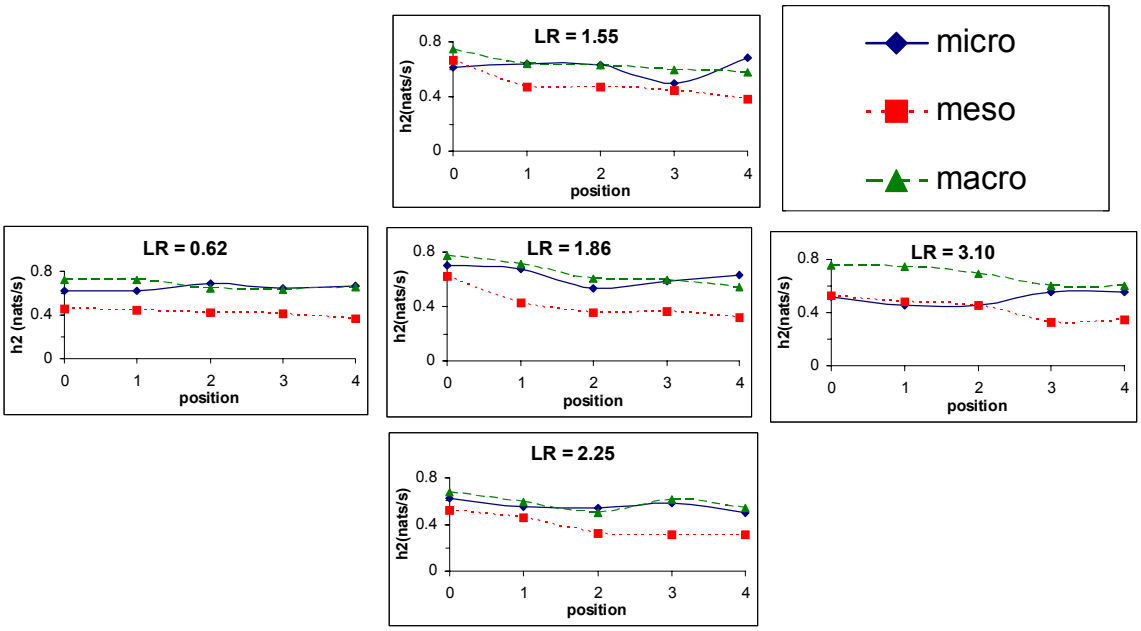

Figure 7- Average correlation entropy versus radial position at the 8.3m elevation for each scale identified with wavelet analysis.

Summary

It has been shown that the raw voltage signal obtained from a fiber optic vector probe has more memory, a more complex attractor, and is more closely related to the Gaussian distribution at the wall of the riser of a CFB when compared to data at the center. These trends become more pronounced for increased load ratio values. Through the analysis of the first minimum of the AMI function, correlation dimension, skewness, and excess kurtosis of the raw signal, boundaries for the flow regimes of dilute upflow to core annular and core annular to fast fluid bed can be identified.

The wavelet decomposition of the raw signal allows for the examination of the micro, meso, and macro scales independently. From this it can be seen that the mesoscale has the greatest influence on the intermittency and dynamics of the raw signal. Also, the influence of this scale is greater at the wall than at the center of the riser.

Acknowledgements

This research was supported in part by an appointment to the National Energy Technology Laboratory Research Participation Program, sponsored by the US Department of Energy and administered by the Oak Ridge Institute for Science and Education.

References

1. Bai, D., H. T. Bi, and J. R. Grace, (1997a). Chaotic Behavior of Fluidized Beds Based on Pressure and Voidage Fluctuations. American Institute of Chemical Engineers Journal, 43, 1357-1361.
2. Briens, L. A., and N. Ellis, (2005). Hydrodynamics of Three-Phase Fluidized Bed Systems Examined by Statistical, Fractal, Chaos and Wavelet Analysis Methods. Chemical Engineering Science, 60, 6094-6106.
3. Cabrejos, F. J., and G. E. Klinzing, (1995). Characterization of Dilute Gas-Solids Flow using the Rescaled Range Analysis. Powder Technology, 84, 139-156.

4. Ellis, N., L. A. Briens, J. R. Grace, H. T. Bi, and C. J. Lim, (2003). Characterization of Dynamic Behavior in Gas-Solid Turbulent Fluidized Bed Using Chaos and Wavelet Analyses. Chemical Engineering Science, 96, 105-116.
5. Fuller, T. A., T. J. Flynn, C. S. Daw, and J. S. Halow, (1993). Interpretation of Pilot-Scale, Fluidized Bed Behavior using Chaotic Time Series Analysis. Proceedings of the 12th International Conference on Fluidized Bed Combustion (pp. 141-153).
6. Goldhirsh, I. (1999). Scales and Kinetics of Granular Flows. Chaos, 9, 659-672.
7. Grassberger, P., and I. Procaccia, (1983). Characterization of Strange Attractors. Physical Review Letters, 50, 346-349.
8. Gu, L.-L., and J.-X. Zhu. Study on Flow Microstructure and Scale up Effect in Circulating Fluidized Bed Risers Using Solids Concentration Signals. Powder Technology, manuscript submitted for publication.
9. Guenther, C., and R. Breault, (2007). Wavelet Analysis to Characterize Cluster Dynamics in a Circulating Fluidized Bed. Powder Technology, 173, 163-173.
10. Hay, J. M., B. H. Nelson, C. L. Briens, and M. A. Bergougnou, (1995). The Calculation of the Characteristics of a Chaotic Attractor in a Gas-Solid Fluidized Bed. Chemical Engineering Science, 50, 373-380.
11. Ji, H., H. Ohara, K. Kuramoto, A. Tsutsumi, K. Yoshida, and T. Hirama, (2000). Nonlinear Dynamics of Gas-Solid Circulating Fluidized-Bed System. Chemical Engineering Science, 55, 403-410.
12. Li, J., and M. Kwauk, (2003). Exploring Complex Systems in Chemical Engineering-The Multi-Scale Methodology. Chemical Engineering Science., 58, 521-535.
13. Monazam, E. R., L. J. Shadle, J. S. Mei, and J. Spenik, (2005). Identification and Characteristics of Different Flow Regimes in a Circulating Fluidized Bed. Powder Technology, 155, 17-25.
14. Tabachnick, B.G., and L. S. Fidell, (1996). Using Multivariate Statistics (3rd ed). New York: Harper Collins.
15. Takens, F. (1981). Detecting strange attractors in Turbulence. In D. A. Rand, & L.-S. Young (Eds.), Lecture notes in mathematics, Dynamical Systems and Turbulence, 898, 366-381. Berlin: Springer.
16. Wu, B., A. Kantzas, C. T. Bellehumeur, Z. He, and S. Kryuchkov, (2007). Multiresolution Analysis of Pressure Fluctuations in a Gas-Solid Fluidized Bed: Application to Glass Beads and Polyethylene Powder Systems. Chemical Engineering Science, 131, 23-33.
17. van den Bleek, C. M., M. O. Coppens, and J. C. Schouten, (2002). Application of Chaos Analysis to Multiphase Reactors. Chemical Engineering Science, 57, 4763-4778.
18. van den Bleek, C. M., and J. C. Schouten, (1993). Deterministic Chaos: A New Tool in Fluidized Bed Design and Operation. The Chemical Engineering Journal, 53, 75-87.
19. Yerushalmi, J., D. H. Turner, and A. M. Squires (1976). The Fast Fluidized Bed. Industrial and Engineering Chemistry Process Design and Development, 15, 47-53.
20. Zhao, G. B., and Y. R. Yang, (2003). Multiscale Resolution of Fluidized-Bed Pressure Fluctuations. American Institute of Chemical Engineers Journal, 49, 869-882.
21. Zinn, A., E. Monazam, J. Spenik, J. Ludlow, (2006). REM Laser Probe Contract Results and Summary. DOE/NETL-2006/1229.